desired state as the ground state. Instead of driving only the blue sideband, we use the Hamiltonian

$$\hat{H}_{+} = \hbar\Omega(\hat{K}^{\dagger}\hat{\sigma}_{+} + \hat{K}\hat{\sigma}_{-}) \quad (3)$$

in which the motional state operators are conjugated with respect to $\hat{H}_{-}$ (Fig. 1C). This results in Rabi oscillations between the states $|\downarrow\rangle|\hat{U}, n\rangle$ and $|\uparrow\rangle|\hat{U}, n+1\rangle$. Because the internal states involved span a two-dimensional Hilbert space, the motional state evolution is also contracted onto two adjacent states of the engineered basis. For an arbitrary initial state, the internal state populations evolve according to Eq. 2, with the corresponding $p(n)$ being the probability of finding the ion in the nth element of the engineered basis before the application of $\hat{H}_{+}$ [we denote this as $p_U(n)$ in the figure to avoid confusion]. Data sets from this type of measurement are shown for the coherent state and for the squeezed state in Fig. 4 for the same settings as used in Figs. 2 and 3. To work in the same basis as the state engineering, we again drive combinations of the carrier and red and blue motional sidebands, but with the ratios of Rabi frequencies calibrated according to $\Omega_c/\Omega_{bsb} = -\alpha^*/\cosh(r)$ and $\Omega_{rsb}/\Omega_{bsb} = e^{-i\phi_s}\tanh(r)$ with ξ and α corresponding to the values used for the reservoir engineering (*16*).

We fit both experimental data sets with a form similar to Eq. 2, obtaining the probability of being found in the ground state of 0.90 ± 0.02 and 0.88 ± 0.02 for the coherent and squeezed states, respectively. We take these to be lower bounds on the fidelity with which these states were prepared, because these numbers include errors in the analysis pulse in addition to state-preparation errors (*16*). The $\hat{H}_{+}$ Rabi oscillations observed in our experiments involve transitions that when viewed in the energy eigenstate basis, couple Hilbert spaces that are of appreciable size. To account for 88% of the populations in oscillations between $|\hat{S}(\xi), 0\rangle$ and $|\hat{S}(\xi), 1\rangle$ for $r = 1.45$, we must include energy eigenstates up to $n = 26$. By our choice of basis, we reduce the relevant dynamics to a two-state system, greatly simplifying the resulting evolution of the spin populations and thus providing a high signal-to-noise ratio. The high fidelity with which the squeezed state is produced is a result of the robust nature of the reservoir engineering, which is insensitive to laser intensity and frequency fluctuations that are common to all frequency components of the engineered Hamiltonian. To generate the same state produced above with standard methods involving unitary evolution starting from the ground state would require simultaneously driving both second motional sidebands (*16*). We would not expect a high fidelity because these have Rabi frequencies comparable to our transition linewidth, which is broadened by magnetic field fluctuations.

This toolbox for generating, protecting, and measuring quantum harmonic oscillator states is transferrable to any physical system in which the relevant couplings can be engineered, facilitating quantum computation with continuous variables (*22*). Examples in which reservoir engineering have been proposed include superconducting circuits and nanomechanics (*12*–*14*). Reservoir engineering provides access to controlled dissipation, which can be used in quantum simulations of open quantum systems (*13*, *23*).

REFERENCES AND NOTES

1. J. I. Cirac, A. S. Parkins, R. Blatt, P. Zoller, *Phys. Rev. Lett.* **70**, 556–559 (1993).
2. J. F. Poyatos, J. I. Cirac, P. Zoller, *Phys. Rev. Lett.* **77**, 4728–4731 (1996).
3. A. R. R. Carvalho, P. Milman, R. L. de Matos Filho, L. Davidovich, *Phys. Rev. Lett.* **86**, 4988–4991 (2001).
4. F. Verstraete, M. M. Wolf, J. I. Cirac, *Nat. Phys.* **5**, 633–636 (2009).
5. S. Diehl *et al.*, *Nat. Phys.* **4**, 878–883 (2008).
6. B. Kraus *et al.*, *Phys. Rev. A* **78**, 042307 (2008).
7. F. Pastawski, L. Clemente, J. I. Cirac, *Phys. Rev. A* **83**, 012304 (2011).
8. H. Krauter *et al.*, *Phys. Rev. Lett.* **107**, 080503 (2011).
9. J. T. Barreiro *et al.*, *Nature* **470**, 486–491 (2011).
10. Y. Lin *et al.*, *Nature* **504**, 415–418 (2013).
11. S. Shankar *et al.*, *Nature* **504**, 419–422 (2013).
12. A. Sarlette, J. M. Raimond, M. Brune, P. Rouchon, *Phys. Rev. Lett.* **107**, 010402 (2011).
13. C. Navarrete-Benlloch, J. J. García-Ripoll, D. Porras, *Phys. Rev. Lett.* **113**, 193601 (2014).
14. A. Kronwald, F. Marquardt, A. A. Clerk, *Phys. Rev. A* **88**, 063833 (2013).
15. W. Schleich, *Quantum Optics in Phase Space* (Wiley-VCH, Berlin, 2001).
16. Materials and methods are available as supplementary materials on *Science* Online.
17. C. Roos, Controlling the quantum state of trapped ions, Ph.D. thesis, Universität Innsbruck, Austria (2000).
18. D. J. Wineland *et al.*, *J. Res. Natl. Inst. Stand. Technol.* **103**, 259 (1998).
19. C. F. Roos, *New J. Phys.* **10**, 013002 (2008).
20. D. M. Meekhof, C. Monroe, B. E. King, W. M. Itano, D. J. Wineland, *Phys. Rev. Lett.* **76**, 1796–1799 (1996).
21. H. P. Yuen, *Phys. Rev. A* **13**, 2226–2243 (1976).
22. D. Gottesman, A. Kitaev, J. Preskill, *Phys. Rev. A* **64**, 012310 (2001).
23. C. J. Myatt *et al.*, *Nature* **403**, 269–273 (2000).

ACKNOWLEDGMENTS

We thank J. Alonso, A. Imamoglu, and D. Wineland for comments on the manuscript and useful discussions. We thank J. Alonso, M. Sepiol, K. Fisher, and C. Flühmann for contributions to the experimental apparatus. We acknowledge support from the Swiss National Science Foundation under grant 200021_134776 and through the National Centre of Competence in Research for Quantum Science and Technology (QSIT).

SUPPLEMENTARY MATERIALS

www.sciencemag.org/content/347/6217/53/suppl/DC1
Supplementary Text
Tables S1 to S3
References (*24*–*28*)

9 September 2014; accepted 24 November 2014
10.1126/science.1261033

ORGANIC CHEMISTRY

Rh-catalyzed C–C bond cleavage by transfer hydroformylation

Stephen K. Murphy,[1,2] Jung-Woo Park,[1] Faben A. Cruz,[1] Vy M. Dong[1]*

The dehydroformylation of aldehydes to generate olefins occurs during the biosynthesis of various sterols, including cholesterol in humans. Here, we implement a synthetic version that features the transfer of a formyl group and hydride from an aldehyde substrate to a strained olefin acceptor. A Rhodium (Xantphos)(benzoate) catalyst activates aldehyde carbon-hydrogen (C–H) bonds with high chemoselectivity to trigger carbon-carbon (C–C) bond cleavage and generate olefins at low loadings (0.3 to 2 mole percent) and temperatures (22° to 80°C). This mild protocol can be applied to various natural products and was used to achieve a three-step synthesis of (+)-yohimbenone. A study of the mechanism reveals that the benzoate counterion acts as a proton shuttle to enable transfer hydroformylation.

The cytochrome P450 enzymes have captured the imagination of chemists who seek to emulate their reactivity. For example, monooxygenases motivated the design of catalysts that epoxidize olefins and oxidize C–H bonds (*1*–*4*). This enzyme superfamily also includes various demethylases that break C–C bonds (*5*). In particular, lanosterol demethylase converts aldehydes to olefins by dehydroformylation during the biosynthesis of sterols in bacteria, algae, fungi, plants, and animals (*6*) (Fig. 1A). Inspired by this step in biosynthesis, we sought a transition-metal catalyst for dehydroformylations in organic synthesis.

[1]Department of Chemistry, University of California Irvine, CA 92697-2025, USA. [2]Department of Chemistry, University of Toronto, Ontario M5S 3H6, Canada.
*Corresponding author. E-mail: dongv@uci.edu

To this end, we aimed to trigger C–C bond cleavage (*7*–*11*) by chemoselective activation of aldehyde C–H bonds using Rh-catalysis (Fig. 1B). Over the past 50 years, activating aldehyde C–H bonds with Rh has been thoroughly investigated (*12*); however, the resulting acyl-Rh^{III}-hydrides have been trapped mainly by hydroacylation (*13*) or decarbonylation (*14*, *15*). This common intermediate is also implicated in hydroformylation, which is practiced on an industrial scale using synthesis gas (*16*). Thus, we needed a strategy for diverting the acyl-Rh^{III}-hydride toward dehydroformylation. To date, olefins generated by dehydroformylation have been observed in low quantities during decarbonylations (*15*, *17*, *18*). One report describes the use of stoichiometric Ru for dehydroformylation of butyraldehyde (*19*), and another uses heterogeneous Rh or Pd catalysts for transforming steroidal aldehydes

at 160 to 300°C (*20*). In contrast, an Fe-peroxo complex cleaves aldehyde C–C bonds at room temperature, but this complex must be used in stoichiometric amounts and can lead to olefin epoxidation (*21*, *22*).

Given this challenge, we designed a strategy in which dehydroformylation of an aldehyde substrate is driven by the concomitant hydroformylation of a strained olefin acceptor (Fig. 1C) (*23*, *24*). This transfer hydroformylation avoids the accumulation of CO gas, which acts as a catalyst poison in related aldehyde dehomologations. Thus, formyl group transfer should proceed under mild conditions. Brookhart's study on the linear-to-branched isomerization of aldehydes with Rh catalysis supports the feasibility of this approach (*25*). Moreover, Morimoto developed hydroformylations of monosubstituted olefins using formaldehyde as a source of CO and H_2 (*26*). Here, we report a Rh catalyst for transfer hydroformylation that operates in the 22° to 80°C temperature range, with loadings as low as 0.3 mole percent (mol %). This mild protocol for dehydroformylation can be applied to a wide range of aldehydes, including those derived from alkaloid, terpene, steroid, and macrolide natural products.

During initial studies, we obtained promising results by investigating nontraditional counterions for Rh(Xantphos) complexes (Fig. 2). The Xantphos ligand was chosen given its success in related hydroacylations, hydroformylations, and decarbonylations (*13*, *16*). Using citronellal (**1a**) and norbornadiene (**5a**) as the model substrate and acceptor, respectively, we observed that typical counterions such as BF_4^- and Cl^- yielded trace decarbonylation products, whereas a softer counterion, I^-, led to mixed dehydroformylation and decarbonylation reactivity. An increase in reactivity and selectivity was obtained by switching to organic counterions such as phenolates and sulfonamidates. The use of a benzoate counterion provided a breakthrough in efficiency. Against expectations, further tuning of the counterion revealed few trends related to acidity, Hammett parameters, or coordinating ability. This observation suggests that the counterion plays a critical role in the mechanism. 3-Methoxybenzoate provided a fivefold increase in initial rate compared with benzoate. We also identified 5-norbornene-2-carboxaldehyde (**6a**) as a stoichiometric product in each of these reactions indicating that a transfer hydroformylation mechanism operates.

The choice of olefin acceptor influences both catalyst loading and reaction temperature (Fig. 2). Because norbornadiene (**5a**) gave selectivity greater than 99:1 **2a**:**3a**, the catalyst loading could be lowered to 0.3 mol % at 80°C or 1 mol % at 60°C using this acceptor. The reaction temperature could be further reduced by using olefin acceptors that cannot chelate to Rh. For instance, norbornene (**5b**) displayed excellent reactivity at 40°C, whereas a slightly more strained acceptor, benzonorbornadiene (**5c**), provided reactivity at ambient temperature. To examine the scope of this strategy, we chose norbornadiene (**5a**) as the acceptor because it afforded the highest chemoselectivity with the lowest catalyst loadings.

This transfer hydroformylation protocol enables access to olefins from a wide range of aldehyde precursors (Fig. 3, A and B). The Diels-Alder cycloaddition was used to generate cyclohexene-4-carboxaldehdye substrates **1b** through **1d**. The trans adduct **1b** underwent dehydroformylation to yield the conjugated 1,3-diene, whereas **1c** gave a mixture of 1,3- and 1,4-dienes. The cis Diels-Alder adduct **1d** yielded the 1,3-diene exclusively, most likely as a result of a syn-selective β-hydride elimination. We reason that the observed regioselectivities are controlled by kinetics because 4-phenylbutanal (**1e**) yields the terminal olefin (**2e**) without any isomerization to the styrene derivative. In general, Lewis basic functionality, such as ethers, esters, amines, phthalimides, and indoles, were tolerated (**1f** to **1i** and **1l**). A vinylindole was derived by dehydroformylation of **1g**, which was ultimately prepared from commercial indole and acrolein. Although 4-pentenals are prototypical substrates for intramolecular olefin hydroacylation, the α-allylated aldehyde **1h** underwent chemoselective dehydroformylation to yield the conjugated diene. Disubstituted olefins enriched in the *E* stereoisomer (>20:1 *E*/*Z*) were accessed from the corresponding α-arylated aldehydes (**1i**). Substrates that do not form conjugated products

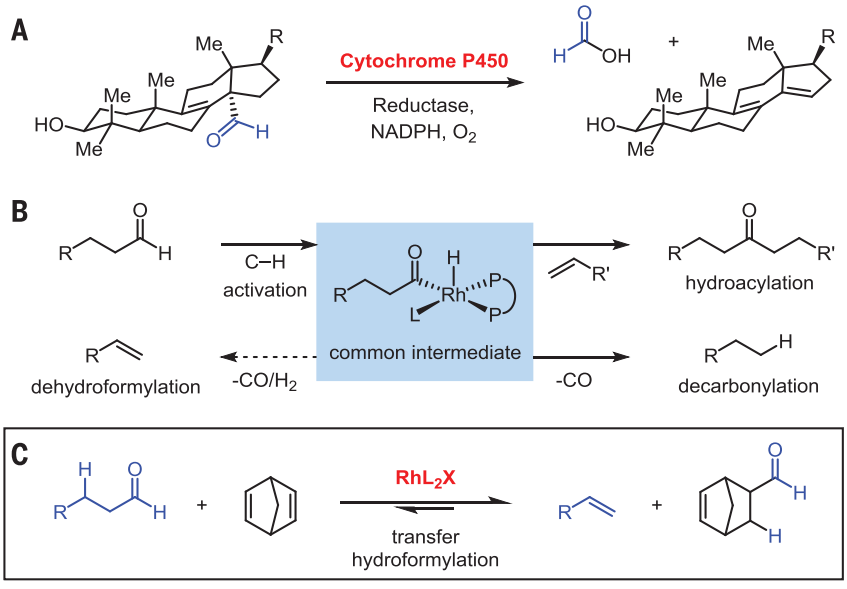

Fig. 1. Dehydroformylation in nature and organic synthesis. (**A**) Dehydroformylation during sterol biosynthesis. (**B**) Reactivity of acyl-Rh^{III}-hydrides. (**C**) Proposed transfer hydroformylation.

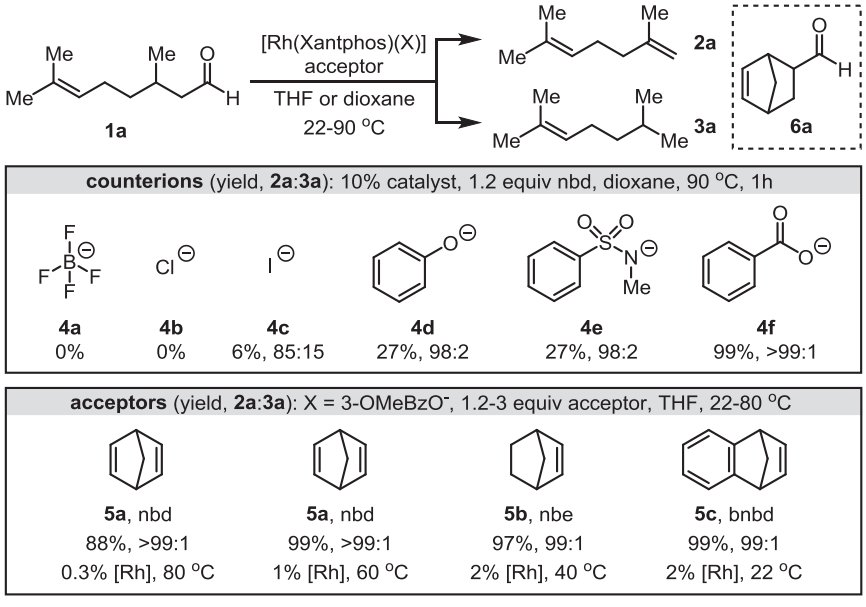

Fig. 2. Effects of counterion structure and ring strain. Yields were determined by gas chromatographic analysis of the reaction mixtures using durene as an internal standard. nbd, norbornadiene; nbe, norbornene; bnbd, benzonorbornadiene.

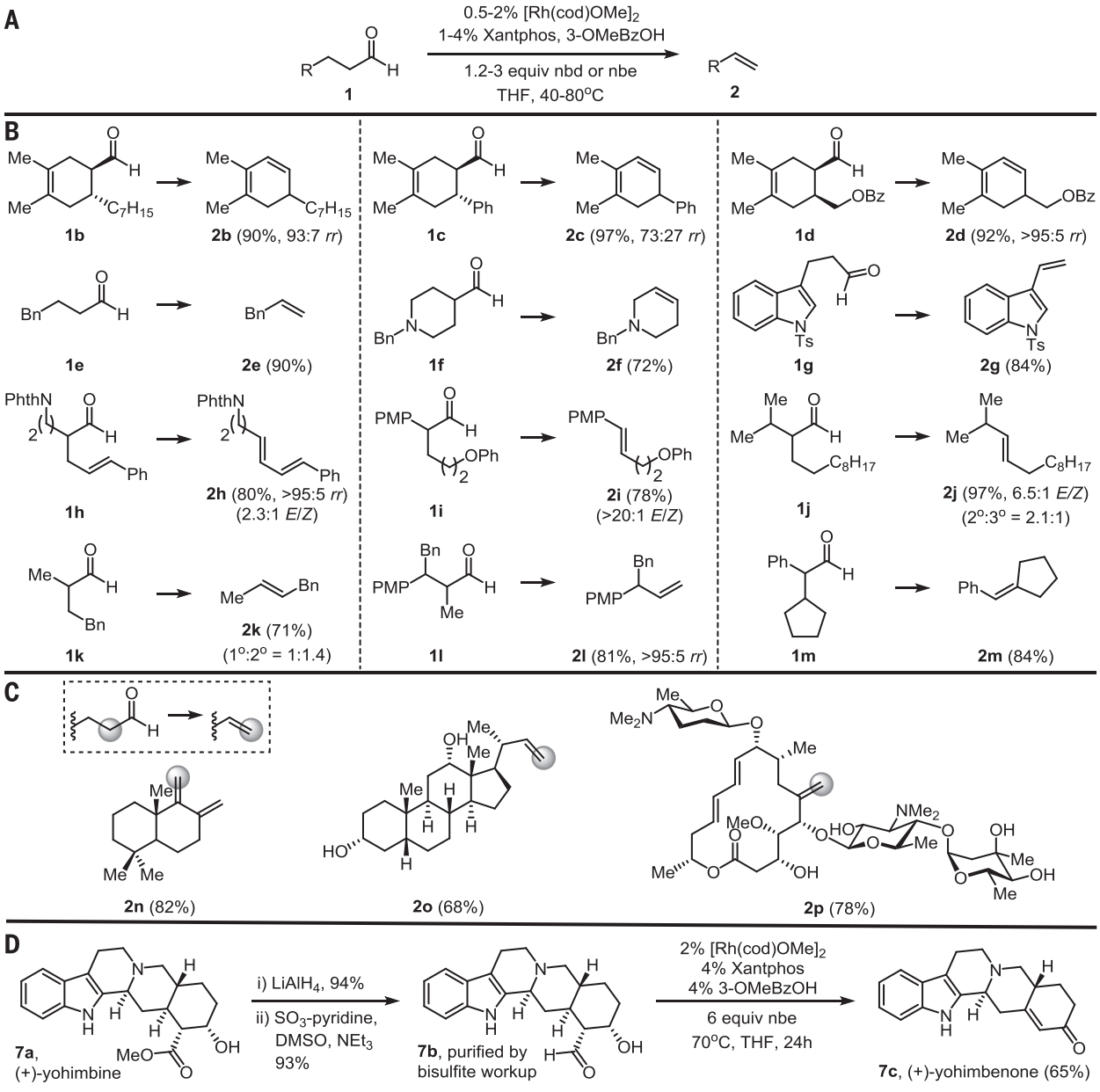

Fig. 3. Applications of dehydroformylation. (**A**) General conditions for transfer hydroformylation. (**B**) Substrate scope. (**C**) Natural product derivatization. (**D**) Three-step synthesis of (+)-yohimbenone. Yields are of isolated materials and mixtures of regioisomers where indicated. *rr* is the regioisomeric ratio; *rr* values were determined by ^{1}H NMR analysis of the reaction mixtures. The yields of **2e** and **2k** were determined by ^{1}H NMR analysis of the reaction mixtures using durene as an internal standard. See the supplementary materials for details.

upon dehydroformylation were transformed with modest regioselectivities (**1j** and **1k**); however, steric congestion favored terminal olefins over trisubstituted products (**1l**). Nonetheless, trisubstituted olefins were generated from substrates containing a single syn-β-hydrogen such as **1m**.

Next, we applied this protocol to generate structurally complex olefins from natural products (Fig. 3C). By dehydroformylation of a (+)-sclareolide derivative, we accessed a carbon-based scaffold **2n** containing an exocyclic diene adjacent to a quaternary center. This product is a key intermediate in the synthesis of several terpenes. Furthermore, (+)-sclareolide is an inexpensive and readily available precursor, whereas typical precursors such as (+)-manool and (−)-polygodial have either been discontinued by commercial suppliers or are available only in milligram quantities (*27*).

To study the chemoselectivity of dehydroformylation, we examined steroid and macrolide substrates (Fig. 3C). Deoxycholic acid derivative **2o** was prepared without protection of the hydroxyl groups, despite the potential for alcohol oxidation under Rh catalysis (*28*, *29*). Thus, activation of the aldehyde C–H bond occurred with high chemoselectivity to initiate C–C bond cleavage. Smooth dehydroformylation of the antibiotic spiramycin I to generate macrolide **2p** highlights the tolerance of this method to many functional groups, including dienes, amines, ethers, esters, and acetals. In this case, dehydroformylation introduced an exocyclic olefin that dramatically altered the topology of the macrolide.

The yohimbinoid family of indole alkaloids has often served as a testing ground for methodology (*30*). Padwa reported the de novo synthesis of racemic yohimbenone in 11 steps from methyl 3-indolylacetate (*31*). By using dehydroformylation as a key step, we prepared (+)-yohimbenone in three steps from commercially available and inexpensive (+)-yohimbine. Conversion of ester **7a** to β-hydroxy aldehyde **7b** was achieved in 87% yield by $LiAlH_4$ reduction followed by

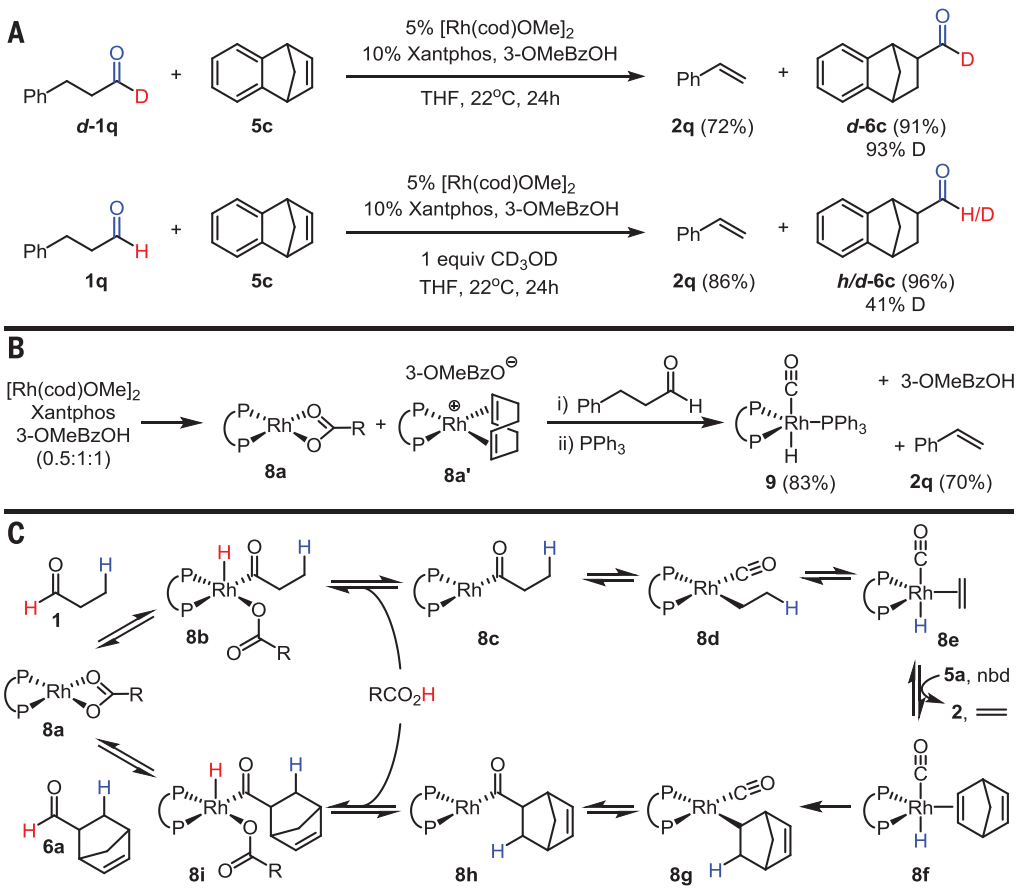

Fig. 4. Mechanistic studies. (**A**) Deuterium labeling studies. (**B**) Isolation of organometallic intermediates. (**C**) Proposed catalytic cycle.

Parikh-Doering oxidation, and the resulting aldehyde was purified by a simple workup with sodium bisulfite. This aldehyde contains both a syn- and an anti-β-hydrogen. Syn-selective dehydroformylation established the trisubstituted olefin at the ring junction. To our surprise, however, the resulting allylic alcohol underwent transfer dehydrogenation in the same pot to yield (+)-yohimbenone in 65% yield. Because dehydroformylation is faster than the allylic alcohol oxidation, either the allylic alcohol or enone product could be selectively formed by controlling the reaction temperature and stoichiometry of the strained olefin acceptor (*32*).

Through experiments designed to probe the mechanism, we obtained insight into why the counterion and strained acceptor are critical in diverting the acyl-Rh^{III}-hydride intermediate along the dehydroformylation pathway. Isotopic labeling studies revealed that the deuterium label of aldehyde ***d*-1q** was incorporated into the formyl group of the product ***d*-6c**. However, statistical scrambling occurred when protio-**1q** was subjected to transfer hydroformylation in the presence of deuterated methanol (Fig. 4A). Together, these results suggest that the aldehyde proton is transferred to the product through the intermediacy of 3-methoxybenzoic acid, which can undergo proton exchange with methanol. Experiments using stoichiometric Rh support this mechanistic scenario (Fig. 4B). Combining the Rh-source, 3-methoxybenzoic acid, and phosphine ligand resulted in an equilibrium mixture of Rh complexes **8a** and **8a′**, each with 3-methoxybenzoate counterions. Upon treatment of this mixture with hydrocinnamaldehyde (**1q**), we observed styrene (**2q**) in high yields along with the regeneration of the benzoic acid derivative (*33*). Subsequent addition of PPh_3 enabled us to identify the organometallic product, Rh-hydrido-carbonyl **9**, which is a catalyst for traditional hydroformylations (*34*). Although stoichiometric dehydroformylation takes place in the absence of the strained acceptor, our studies on the catalytic process revealed a correlation between the ring strain of the acceptor and the selectivity for dehydroformylation versus decarbonylation. Therefore, we propose that stoichiometric dehydroformylation in the absence of acceptor is thermodynamically downhill and reversible, but norbornadiene can irreversibly trap the Rh-hydrido-carbonyl intermediate to prevent decarbonylation and turn over the catalyst.

A proposed catalytic cycle for transfer hydroformylation is depicted in Fig. 4C. The neutral Rh complex **8a** activates the aldehyde C–H bond to generate acyl-Rh^{III}-hydride **8b**. The 3-methoxybenzoate counterion can then undergo reductive elimination with the hydride ligand to generate acyl-Rh^{I} **8c** and 3-methoxybenzoic acid (*35*). In contrast, most hydroacylations and decarbonylations typically employ innocent counterions such as Cl^- and BF_4^-. De-insertion of CO and subsequent β-hydride elimination forges Rh-hydrido-carbonyl **8e**. Exchange of the olefin product with norbornadiene (**5a**) generates **8f**, which irreversibly leads to the transfer hydroformylation product **6a** through similar mechanistic steps in reverse order (Fig. 4C). Thus, the ring strain of the olefin acceptor and the ability of the counterion to act as a proton shuttle by reversible redox processes afford high reactivity and selectivity.

REFERENCES AND NOTES

1. J. T. Groves, *Proc. Natl. Acad. Sci. U.S.A.* **100**, 3569–3574 (2003).
2. R. Breslow, Y. Huang, X. Zhang, J. Yang, *Proc. Natl. Acad. Sci. U.S.A.* **94**, 11156–11158 (1997).
3. M. S. Chen, M. C. White, *Science* **327**, 566–571 (2010).
4. W. Zhang, J. L. Loebach, S. R. Wilson, E. N. Jacobsen, *J. Am. Chem. Soc.* **112**, 2801–2803 (1990).
5. A. Sigel, H. Sigel, R. K. O. Sigel, Eds., *The Ubiquitous Roles of Cytochrome P450 Proteins: Metal Ions in Life Sciences*, vol. 3 (Wiley, New York, 2007).
6. G. I. Lepesheva, M. R. Waterman, *Biochim. Biophys. Acta* **1770**, 467–477 (2007).
7. A. Dermenci, J. W. Coe, G. Dong, *Org. Chem. Front.* **1**, 567–581 (2014).
8. C.-H. Jun, *Chem. Soc. Rev.* **33**, 610–618 (2004).
9. H. M. Ko, G. Dong, *Nat. Chem.* **6**, 739–744 (2014).
10. Z. Zuo *et al.*, *Science* **345**, 437–440 (2014).
11. Y. Liu *et al.*, *Adv. Synth. Catal.* **356**, 130–136 (2014).
12. M. A. Garralda, *Dalton Trans.* **2009**, 3635–3645 (2009).
13. M. C. Willis, *Chem. Rev.* **110**, 725–748 (2010).
14. J. Tsuji, K. Ohno, *Tetrahedron Lett.* **6**, 3969–3971 (1965).
15. M. Kreis, A. Palmelund, L. Bunch, R. Madsen, *Adv. Synth. Catal.* **348**, 2148–2154 (2006).

16. R. Franke, D. Selent, A. Börner, *Chem. Rev.* **112**, 5675–5732 (2012).
17. T. Iwai, T. Fujihara, Y. Tsuji, *Chem. Commun.* **2008**, 6215–6217 (2008).
18. T. Kondo, M. Akazome, Y. Tsuji, Y. Watanabe, *J. Org. Chem.* **55**, 1286–1291 (1990).
19. R. H. Prince, K. A. Raspin, *Chem. Commun.* (*London*) **1966**, 156–157 (1966).
20. C. A. McCombs, C. H. Foster, Eastman Kodak Company, Dehydroformylation of steroidal aldehydes. U.S. Patent 4272444 A, 14 August 1980.
21. D. L. Wertz, M. F. Sisemore, M. Selke, J. Driscoll, J. S. Valentine, *J. Am. Chem. Soc.* **120**, 5331–5332 (1998).
22. Y. Goto, S. Wada, I. Morishima, Y. Watanabe, *J. Inorg. Biochem.* **69**, 241–247 (1998).
23. R. Ahuja *et al*., *Nat. Chem.* **3**, 167–171 (2011).
24. D. H. T. Phan, K. G. M. Kou, V. M. Dong, *J. Am. Chem. Soc.* **132**, 16354–16355 (2010).
25. C. P. Lenges, M. Brookhart, *Angew. Chem. Int. Ed.* **38**, 3533–3537 (1999).
26. G. Makado *et al*., *Adv. Synth. Catal.* **352**, 299–304 (2010).
27. M. Cortés, J. A. Valderrama, M. Cuellar, V. Armstrong, M. Preite, *J. Nat. Prod.* **64**, 348–349 (2001).
28. H. Imai, T. Nishiguchi, K. Fukuzumi, *J. Org. Chem.* **39**, 1622–1627 (1974).
29. C.-H. Jun, C.-W. Huh, S.-J. Na, *Angew. Chem. Int. Ed.* **37**, 145–147 (1998).
30. T. P. Lebold *et al*., *Nat. Chem.* **5**, 126–131 (2013).
31. C. J. Stearman, M. Wilson, A. Padwa, *J. Org. Chem.* **74**, 3491–3499 (2009).
32. For detailed experimental conditions, see the supplementary materials on *Science* Online.
33. The peaks for the regenerated benzoic acid are very broad in the nuclear magnetic resonance (NMR) spectra, possibly due to reversible reductive elimination. Analogous results were obtained using 4-fluorobenzoic acid as a surrogate, which enabled us to follow the reaction by ^{19}F NMR and confirm the results.
34. M. Kranenburg *et al*., *Organometallics* **14**, 3081–3089 (1995).
35. M. Manger, J. Wolf, M. Teichert, D. Stalke, H. Werner, *Organometallics* **17**, 3210–3221 (1998).

ACKNOWLEDGMENTS

The authors are grateful for financial support provided by the NIH's National Institute of General Medical Sciences (GM105938). S.K.M. is grateful for a Canada Graduate Scholarship from the Natural Sciences and Engineering Research Council of Canada. We acknowledge C. M. Rathbun for contributions during the optimization stage of reaction development.

SUPPLEMENTARY MATERIALS

www.sciencemag.org/content/347/6217/56/suppl/DC1
Materials and Methods
Supplementary Text
References (*36*–*54*)

15 September 2014; accepted 6 November 2014
10.1126/science.1261232

REACTION DYNAMICS

Extremely short-lived reaction resonances in Cl + HD (v = 1) → DCl + H due to chemical bond softening

Tiangang Yang,[1,2]* Jun Chen,[1]* Long Huang,[1] Tao Wang,[1] Chunlei Xiao,[1]† Zhigang Sun,[1,3]† Dongxu Dai,[1] Xueming Yang,[1,3]† Dong H. Zhang[1,3]†

The Cl + H_2 reaction is an important benchmark system in the study of chemical reaction dynamics that has always appeared to proceed via a direct abstraction mechanism, with no clear signature of reaction resonances. Here we report a high-resolution crossed–molecular beam study on the Cl + HD (v = 1, j = 0) → DCl + H reaction (where v is the vibrational quantum number and j is the rotational quantum number). Very few forward scattered products were observed. However, two distinctive peaks at collision energies of 2.4 and 4.3 kilocalories per mole for the DCl (v' = 1) product were detected in the backward scattering direction. Detailed quantum dynamics calculations on a highly accurate potential energy surface suggested that these features originate from two very short-lived dynamical resonances trapped in the peculiar H-DCl (v' = 2) vibrational adiabatic potential wells that result from chemical bond softening. We anticipate that dynamical resonances trapped in such wells exist in many reactions involving vibrationally excited molecules.

Reaction resonances are quasi-trapped quantum states in the transition state region that profoundly influence both the rate and product distribution of a chemical reaction (*1*–*3*). Since the landmark theoretical predictions of reaction resonances in the H/F + H_2 reaction in the early 1970s (*4*, *5*), extensive studies have been carried out to detect the resonances experimentally and to elucidate them theoretically. However, direct observations have proven to be extremely challenging. Through a series of crossed–molecular beam experiments (*6*–*9*), a physical picture of reaction resonances in F + H_2 (HD) beyond chemical accuracy has been established. In addition, threshold photodetachment spectroscopy has been used to probe resonances in the I + HI reaction (*10*). Recently, resonance signatures have also been detected in polyatomic reactions (*11*–*14*). Forward scattering of reaction products in crossed-beam scattering experiments can be caused by long-lived resonances. However, the presence of forward scattering does not necessarily imply that there are resonances in a chemical reaction. An intriguing question then is if and how we can probe reaction resonances in systems that show no or little forward scattering product, in which the reaction intermediate is very short lived.

Here we report a combined high-resolution crossed-beam and accurate quantum reaction dynamics study on the Cl + HD (v = 1, j = 0) → DCl + H reaction (v, vibrational quantum number; j, rotational quantum number). Our study provides very strong evidence for the existence of short-lived quantum dynamical resonances in this reaction. The Cl + H_2 system has served as one of the most important benchmark systems in the study of chemical reaction dynamics (*15*), along with the H + H_2 and F + H_2 reactions. It has also played a special role in development of the transition state theory and in the verification of kinetic isotope effects (*16*–*19*). In contrast to the F + H_2 reaction, the Cl + H_2 (v = 0) reaction was shown to be a direct abstraction with a colinear later reaction barrier (*20*–*25*).

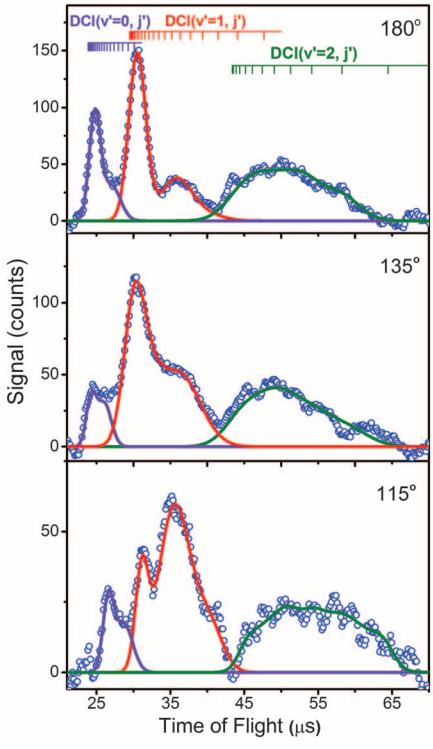

Fig. 1. Time-of-flight spectra of the H atom product from the Cl + HD (v = 1, j = 0) → DCl (v') + H reaction at the collision energy of 4.3 kcal/mol at different laboratory angles.

[1]State Key Laboratory of Molecular Reaction Dynamics, Dalian Institute of Chemical Physics, Chinese Academy of Sciences, Dalian, Liaoning 116023, China. [2]School of Physics and Optoelectric Engineering, Dalian University of Technology, Dalian, Liaoning 116023, China. [3]Center for Advanced Chemical Physics and 2011 Frontier Center for Quantum Science and Technology, University of Science and Technology of China, 96 Jinzhai Road, Hefei 230026, China.
*These authors contributed equally to this work. **†Corresponding author. E-mail: chunleixiao@dicp.ac.cn (C.X.); zsun@dicp.ac.cn (Z.S.); xmyang@dicp.ac.cn (X.Y.); zhangdh@dicp.ac.cn (D.H.Z.)**

Rh-catalyzed C–C bond cleavage by transfer hydroformylation

Stephen K. Murphy *et al.*

Science **347**, 56 (2015);
DOI: 10.1126/science.1261232